Journal of Astronomical Telescopes, Instruments, and Systems

AstronomicalTelescopes.SPIEDigitalLibrary.org

Performance testing of an off-plane reflection grating and silicon pore optic spectrograph at PANTER

Hannah Marlowe
Randall L. McEntaffer
Ryan Allured
Casey T. DeRoo
Benjamin D. Donovan
Drew M. Miles
James H. Tutt
Vadim Burwitz
Benedikt Menz
Gisela D. Hartner
Randall K. Smith
Peter Cheimets
Edward Hertz
Jay A. Bookbinder
Ramses Günther
Alex Yanson
Giuseppe Vacanti
Marcelo Ackermann

Performance testing of an off-plane reflection grating and silicon pore optic spectrograph at PANTER

Hannah Marlowe,[a,*] Randall L. McEntaffer,[a] Ryan Allured,[b] Casey T. DeRoo,[a] Benjamin D. Donovan,[a] Drew M. Miles,[a] James H. Tutt,[a] Vadim Burwitz,[c] Benedikt Menz,[c] Gisela D. Hartner,[c] Randall K. Smith,[b] Peter Cheimets,[b] Edward Hertz,[b] Jay A. Bookbinder,[d] Ramses Günther,[e] Alex Yanson,[e] Giuseppe Vacanti,[e] and Marcelo Ackermann[f]

[a]University of Iowa, Department of Physics & Astronomy, 210 Van Allen Hall, Iowa City, Iowa 52242, United States
[b]Harvard-Smithsonian Center for Astrophysics, 60 Garden Street, Cambridge, Massachusetts 02138, United States
[c]MPI für extraterrestrische Physik, Giessenbachstrasse 1, D-85748 Garching, Germany
[d]NASA Ames Research Center, Moffett Field, California 94035, United States
[e]Cosine Science & Computing BV, J.H. Oortweg 19, 2333 CH Leiden, The Netherlands
[f]Cosine Research BV, J.H. Oortweg 19, 2333 CH Leiden, The Netherlands

Abstract. An x-ray spectrograph consisting of aligned, radially ruled off-plane reflection gratings and silicon pore optics (SPO) was tested at the Max Planck Institute for Extraterrestrial Physics PANTER x-ray test facility. SPO is a test module for the proposed Arcus mission, which will also feature aligned off-plane reflection gratings. This test is the first time two off-plane gratings were actively aligned to each other and with an SPO to produce an overlapped spectrum. We report the performance of the complete spectrograph utilizing the aligned gratings module and plans for future development. [DOI: 10.1117/1.JATIS.1.4.045004]

Keywords: diffraction; gratings; grazing incidence; x-rays.

Paper 15040P received Jun. 2, 2015; accepted for publication Nov. 23, 2015; published online Dec. 22, 2015.

1 Introduction

Arcus[1] is a proposed x-ray spectrograph to be installed on the International Space Station. This spectrograph consists of silicon pore optics (SPOs)[2] and blazed, radially ruled off-plane reflection gratings optimized for the feature-rich soft x-ray regime. The mission will utilize the SPOs being developed for ESA's Athena mission by cosine Research and reflection gratings being developed in collaboration between the University of Iowa and MIT/Lincoln Labs. The Arcus mission will answer key science questions related to structure formation in the Universe, supermassive black hole feedback, and stellar life cycles. To meet its science objectives, Arcus will have a resolution of $\lambda/\Delta\lambda > 2000$ and effective area >400 cm^2 in the critical science bandpass around the O VII and O VIII lines (22.6 to 25 Å). The mission will have a minimum resolution and effective area of $\lambda/\Delta\lambda > 1300$ and >130 cm^2 over the entire bandpass (8 to 52 Å) with $\lambda/\Delta\lambda$ reaching $\sim$3000 at the longest wavelengths.

Performance testing of aligned, off-plane reflection gratings with an SPO module was carried out at the PANTER[3] test facility of the Max Planck Institute for Extraterrestrial Physics in October 2014. During the tests, two radially ruled, laminar profile, off-plane reflection gratings were aligned to the SPO test module. The gratings used in this test were developed at the University of Iowa and are detailed in Ref. 4. This test was the first time that off-plane diffraction gratings were aligned with an SPO and two off-plane gratings were aligned to one another *in situ* to produce an overlapped spectrum. This paper describes the performance of the spectrograph composed of an SPO module and the aligned gratings module. The line spread function (LSF) of the spectrograph, the line widths of the SPO module alone, and the −1st-order Mg-K line of the complete spectrograph are compared. While not covered in depth here, comprehensive detail of the alignment methodology and results will be given in Ref. 5. This paper is organized as follows: the components of the spectrograph are detailed in Sec. 2, a brief overview of the alignment procedure is given in Sec. 3, CCD image reduction steps and measured line widths are presented in Sec. 4, and a discussion of the results is given in Sec. 5.

2 Spectrograph Assembly

The spectrograph assembly tested at the PANTER facility consists of an SPO telescope, off-plane reflection gratings, and a CCD detector at the grating focal plane. A schematic of the SPO, grating, and focal plane positions within the test chamber is shown in Fig. 1. An image of the components installed in the PANTER vacuum chamber during initial grating alignment with a laser is presented in Fig. 2.

2.1 *Silicon Pore Optics*

SPOs have been developed for the past 10 years by a consortium led by cosine Research and have become the main technology for the x-ray mirror of the Athena mission.[6] SPOs make use of industry-standard superpolished silicon wafers. These wafers are first diced into mirror plates of the desired rectangular shape. Then each plate is wedged so that a focusing optic is formed when multiple plates are stacked onto a conical mandrel. Before being stacked, the plates are ribbed, leaving a thin

*Address all correspondence to: Hannah Marlowe, E-mail: hannah-marlowe@uiowa.edu

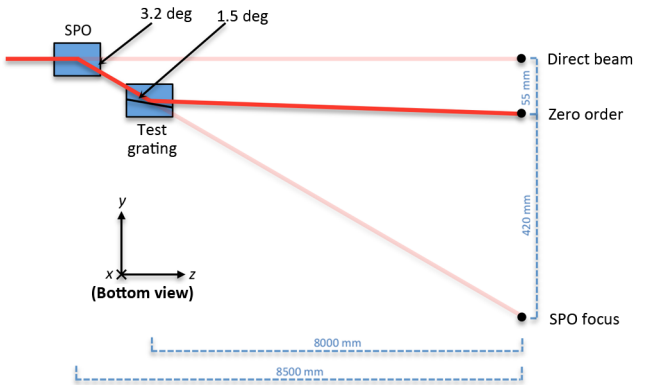

Fig. 1 Block diagram of the test chamber silicon pore optics (SPO) and grating integration.

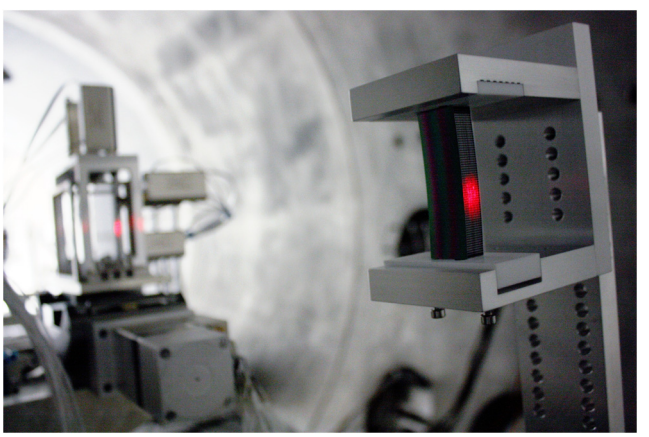

Fig. 2 The SPO as viewed from the source direction during optical alignment. The active alignment grating module is visible in the background.

membrane on one side used to reflect the x-rays and a number of ribs on the other that are used to bond to the next plate. This results in pores in the SPO stack, through which the x-rays can reflect and travel to the focal plane detector. Plates may also be coated to increase their reflectivity. An SPO stack is very stiff and lightweight, and the stacking process is such that the figure of the mandrel is reproduced with high fidelity.

For this campaign, a single SPO stack was built. The stack consists of 13 plates, with radii of curvature between 450 and 439 mm (11 mm in the radial direction), width of 66 mm, and length along the optical axis of 22 mm. Its geometry approximates that of a parabolic reflector in a Wolter I style optic. With a focal length of 8.5 m (for the source distance at the PANTER facility), the wedge on each plate was tuned to deliver the required 10 arc second change in grazing incidence angle between consecutive plates, resulting in a confocal system. For on-axis measurements, the incidence angle is ~1.6 deg. During these tests, a mask was used to illuminate only the inner 66% of the SPO stack in the azimuthal direction.

The SPO stack is shown in Fig. 3 prior to installation in the PANTER vacuum chamber. Due to time and budget constraints, the SPO module for this test was shaped using a simple aluminum mandrel rather than one made of high-quality polished fused silica. Therefore, it is important to note that while similar to the planned Arcus design in focal length and radii, the performance of this SPO module is not characteristic of the state of the art in SPO manufacturing.

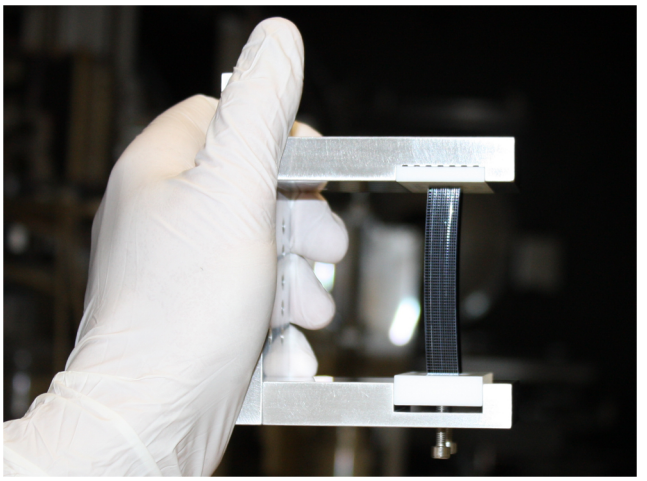

Fig. 3 The SPO module prior to installation in the PANTER chamber.

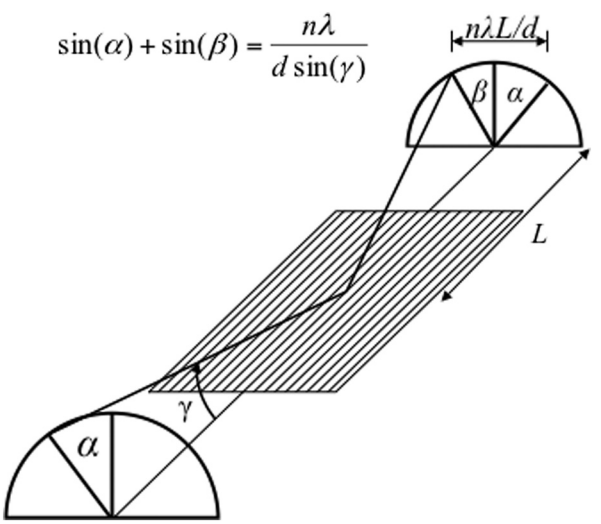

Fig. 4 Geometry of the off-plane grating mount.[4]

2.2 *Gratings*

A diagram of the off-plane grating geometry is shown in Fig. 4. In the off-plane mount, light that is incident onto the gratings at a grazing angle and roughly parallel to the groove direction is diffracted into an arc. The diffraction equation for the off-plane mount is

$$\sin\alpha+\sin\beta=\frac{n\lambda}{d\sin\gamma}, \tag{1}$$

where γ is the polar angle of the incident x-rays defined from the groove axis at the intersection point, d is the line spacing of the grooves, α represents the azimuthal angle along a cone with half-angle γ, and β is the azimuthal angle of the diffracted light. The gratings tested at PANTER have a laminar (rectangular) groove profile and average groove spacing of 6033 grooves/mm. The grating substrates are $100\times100\times0.7$ mm^3 Si wafers with a central grooved area of 25×32 mm^2, where the long dimension is in the optical axis. The grooves are radially ruled such that the spacing between adjacent grooves decreases toward the focus to match the convergence of the telescope, described in detail by McEntaffer et al.[4]

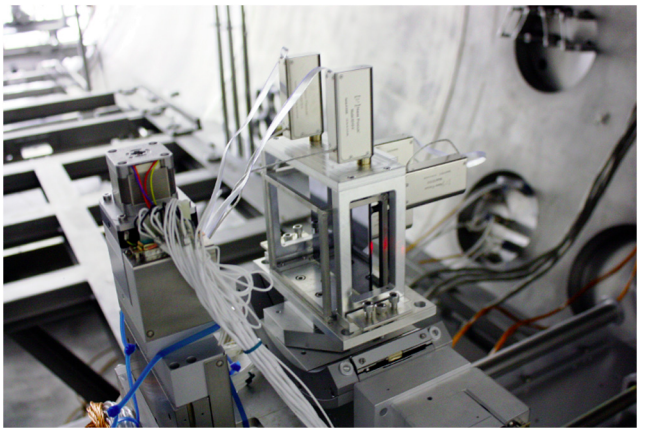

Fig. 5 The active alignment module (AAM) as viewed from the x-ray source direction. The top two picomotors control the active grating yaw, while the three motors on the face of the grating (image right) actuate roll and pitch. The gratings are partially visible in the center of the AAM standing on their sides.

For this test, two gratings were actively aligned together to demonstrate a technique for aligning nested diffraction gratings in an active alignment module (AAM). The AAM consists of slots for the grating wafers and an exterior skeleton into which five picomotors are mounted in order to align sequential gratings to an initially installed, fixed reference grating. The AAM is shown in Fig. 5, where two of the five picomotors, which are used to control grating yaw, are visible on the top of the module and three motors are partially visible on the front of the module, which control pitch and roll actuation of the active grating. The step size of each picomotor is ~30 nm, which translates to angular step sizes of ~0.1 arc second in roll, pitch, and yaw. For this test, only one additional grating was installed and aligned to the reference grating, though the procedure could be repeated to add more gratings as desired. For an incidence angle of 1.5 deg, the two grating AAM stack intercepts 25 mm of the 44 mm (57%) illuminated azimuthal extent of the SPO and 3 mm of the 11 mm (27%) radial extent of the SPO, or ~15% of the total SPO beam. For the remainder of this paper, the AAM will refer to the entire module once the active grating was aligned with the reference grating and bonded into place, and the picomotors and springs were disengaged.

2.3 *Detectors*

Three detectors were in use at the focal plane in the PANTER chamber during this test, TRoPIC, the ROSAT position sensitive proportional counter (PSPC),[7] and PIXI. TRoPIC is a single photon counting detector with 75 μm pixels operated in frame-store mode. TRoPIC is a prototype of the eROSITA detector and is identical apart from its smaller format of 256 × 256 compared to 384 × 384 and a lower operating temperature of $\sim -100^{\circ}$C.[8] The PANTER facility also has a spare of the ROSAT PSPC detector, which we utilized for macro imaging of orders and for rough alignment due to its large active area (80 mm diameter) though relatively course spatial resolution of ~250 μm.[9,10] PIXI is a Peltier and water cooled Princeton Instruments PI-MTE-1300B integrating in-vacuum CCD with 20 μm pixels in a 1340 × 1300 format.[3] All three detectors are shown in Fig. 6. PSPC and TRoPIC are mounted onto the same translation stages and were able to image the 0 and ±1st orders. PIXI was mounted on a separate vertical translation stage sharing the other movements with TRoPIC and PSPC and was able to reach negative orders. This paper focuses on data obtained with the PIXI detector.

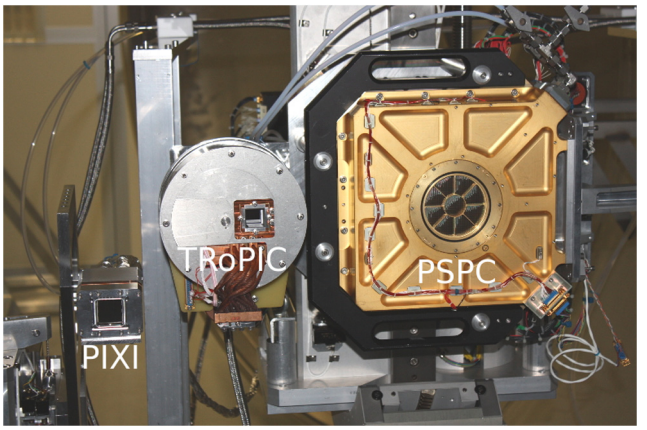

Fig. 6 The x-ray detectors at the PANTER facility. From left to right: PIXI, TRoPIC, and ROSAT position sensitive proportional counter (PSPC).

3 PANTER Testing

To investigate the performance of the spectrograph, the gratings and SPO were installed into the detector chamber of the PANTER test facility. The PANTER beamline consists of a multitarget electron impact x-ray source at the head of a 1 m diameter, 120 m long vacuum chamber. The beamline ends in a 3.5 m by 12 m test chamber, which easily accommodates the SPO, gratings, and detectors.

The gratings were mounted into the PANTER chamber within the AAM with five degrees of freedom relative to the SPO and CCD. In the coordinate space of Fig. 1, the z position was set based on initial physical positioning and verified by laser distance measurement. Linear translation stages in the x and y directions were used to position the grating module into the x-ray beam. A goniometer stage was used to control grating yaw, and a rotation stage controlled pitch. Roll alignment of the gratings was set via mechanical tolerance within the mount. All of the grating module stages were controllable outside of the vacuum chamber. The SPO light is incident on the gratings at an angle of 1.5 deg. This incidence angle was set using the separation between the SPO focus and the zeroth-order reflection of an optical laser mounted at the head of the beamline and has an uncertainty of ~1 cm over the 8 m throw (~4 arc min). The chamber was then evacuated, and the PSPC was used to find the various diffraction orders and to initially zero the reference grating yaw. A mosaic image of the diffraction orders taken by the PSPC detector is shown in Fig. 7. In the mosaic, the active and reference gratings are purposely offset in pitch to illustrate both gratings, and the image is labeled with the various observable diffraction orders. We note that ±3rd-order Mg-K was also visible with the PIXI detector, though it is not within the spatial extent of the PSPC mosaic. The reader will observe that the efficiency in orders is symmetric about the zeroth order. This is due to the current test gratings having laminar rather than blazed groove profiles. For blazed gratings, the efficiency would be biased on a single side of the zeroth order, thus increasing signal-to-noise in those orders. The scatter observed around the zeroth order is attributed to residual specular reflection off of the semitransparent wafer tape on the nonactive region of the gratings.

Of the lines observed, Mg-K has the narrowest natural line width of $(\Delta E/E^{\text{peak}} = 0.36 \text{ eV}/1254 \text{ eV})$[11,12] compared

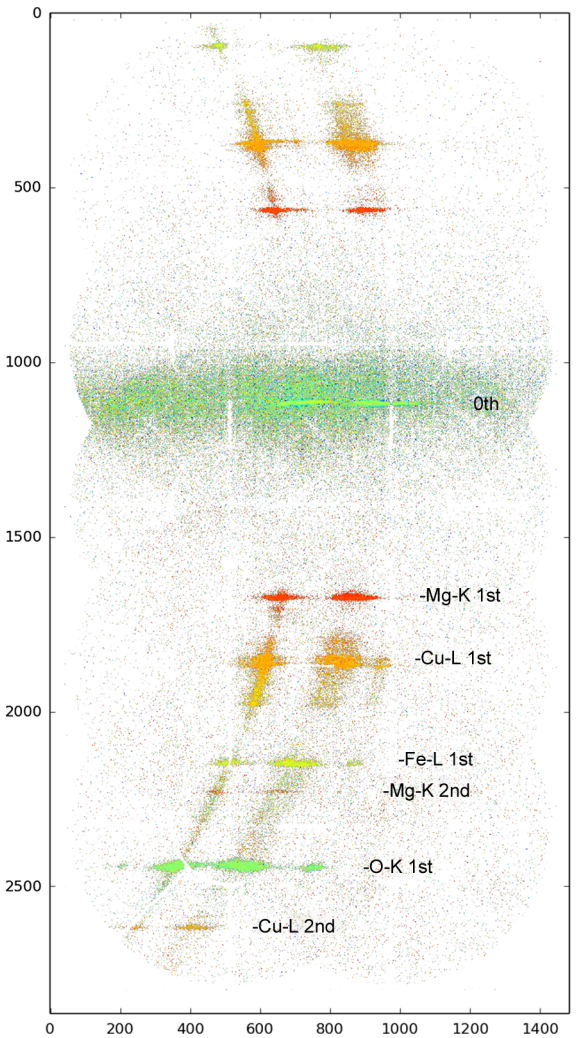

Fig. 7 A mosaic image of the diffraction orders from an Mg target taken by the PSPC detector. The color scale indicates energy, which decreases in the dispersion direction from zeroth order. The image is plotted in a log scale to bring out the individual lines, which are labeled on the right-hand side of the image, and the *x* and *y* units are PSPC pixels.

to Cu-L (3.5 eV/930 eV), O-K (6 eV/525 eV), and Fe-L (3.5 eV/705 eV). However, these line widths are theoretical values, and we note that solid target x-ray sources may include additional broadening effects. Experimental results[13] suggest that in this case, Mg-K may be broadened to 1.1 eV (FWHM). We address this potential contribution to the spectrograph line width in Sec. 5. The best statistics were achieved in the ±1st-order Mg-K line compared with the lower count-rate, higher orders. The relative order efficiencies for these gratings are presented in Ref. 4, demonstrating the large difference in efficiency among the ±1st, ±2nd, and ±3rd orders at the Mg-K energy. Although we observed some small flux from the −2nd and −3rd orders, due to time limitations of the test campaign, we obtained high statistic observations of only the −1st-order Mg-K line, whose LSF we use to characterize the spectrograph performance.

4 Reduction and Resolution

This section outlines the reduction steps taken to extract LSF measurements from the CCD images taken at PANTER.

To process the raw PIXI images, a dark frame is first subtracted from the integrated image. The dark frame is a 1340 × 1300 array whose pixels are the median value of N dark exposures taken consecutively. The dark frames are taken at the same position with the same exposure duration and close in time to the observation frames. The dark-corrected background is characterized by two background regions of the same size but spatially offset from the observation extraction region. The dark-corrected images are thresholded by setting to zero any pixels that fall below three times the background σ value. It is important to note that PIXI is not a photon counting detector and that the result of this processing is an image whose pixels represent (corrected) integrated analog-to-digital units (ADU).

To calculate the dispersion direction LSF, the image is first collapsed in the cross-dispersion direction. However, the SPO focus is asymmetric and is much wider in the cross-dispersion direction compared to the dispersion direction. Thus, any misalignment with respect to the CCD x and y directions would broaden the apparent LSF. Therefore, the image is rotated via a rotation matrix to account for any misalignment with the CCD prior to collapsing in the cross-dispersion direction. The applied rotation angle is found by performing a least squares fit of the form $u = mv + b$, where u is in the dispersion direction, to the image weighted by each pixel value. Such a fit is illustrated in Fig. 8. The applied rotation angle is the one that minimizes the slope of the spectral line with respect to the CCD axis as illustrated in Fig. 9, where the fitted slopes are plotted versus an array of rotation angles. The best rotation is found as the intercept of this linear relationship where the fitted slope is 0, indicated in the plot by a dashed horizontal line.

Figure 10 shows the cropped and rotated PIXI image and projections of the SPO focus before grating installation. The point spread function (PSF) of a grazing incidence x-ray telescope is dominated by figure error and by scatter, with the scattering contribution being greatest in the in-plane reflection direction. For a full 360-deg optic, the PSF is circular with a bright, dense core surrounded by scatter dominated wings.[14] The PSF can be limited in a preferred direction by subaperturing the incident light, creating a focus that is narrow in the chosen direction. The effect of subaperturing for the test module is apparent in Fig. 10, where the focus is much broader in the in-plane direction of the SPO contrasted with a narrow focus in the off-plane (grating dispersion) direction. The LSF of the spectrograph is dominated by the extent of the PSF in the dispersion direction and is limited by the telescope focus in addition to aberrations added by the gratings.

The rotated CCD image is collapsed in the cross-dispersion direction, and the resulting line width characterizes the LSF of the telescope. The SPO focus is not well described by a simple Gaussian model. Therefore, to avoid relying on an underlying

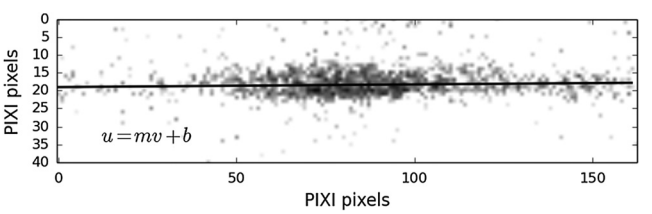

Fig. 8 Least squares fit of the form $u = mv + b$ (where u is in the dispersion direction) applied to the image weighted by each pixel value.

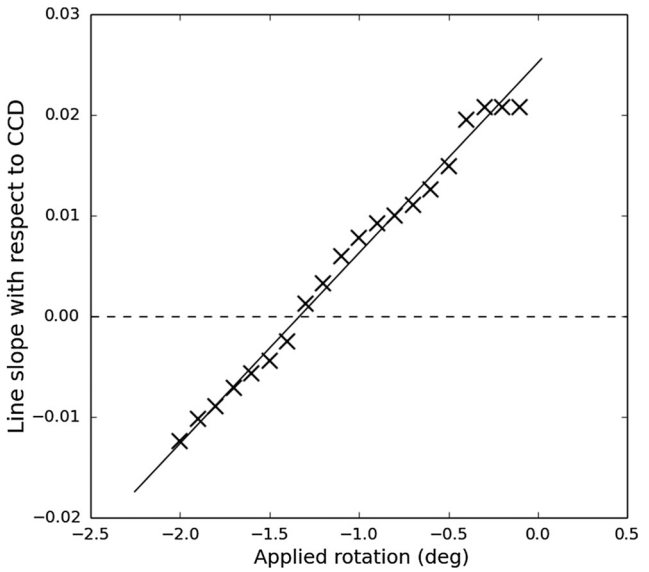

Fig. 9 Slope of the spectral line with respect to the CCD axis versus applied rotation.

distribution, the line width is described in this paper by the half-energy width (HEW) in the dispersion direction, where the HEW contains the central 50% of the line's integrated counts as calculated from its cumulative distribution function (CDF). A spline interpolation is applied to the CDF points, allowing the HEW boundaries to fall between pixel values. The spline interpolated CDF of the SPO focus is shown in Fig. 11, where the vertical dash-dot lines indicate the upper and lower HEW bounds. The HEW is converted to arc seconds from the 20 μm pixels using the focal lengths of the SPO (8.5 m) and gratings (8 m), resulting in conversion factors of 0.49 and 0.52 arc second/pixel, respectively.

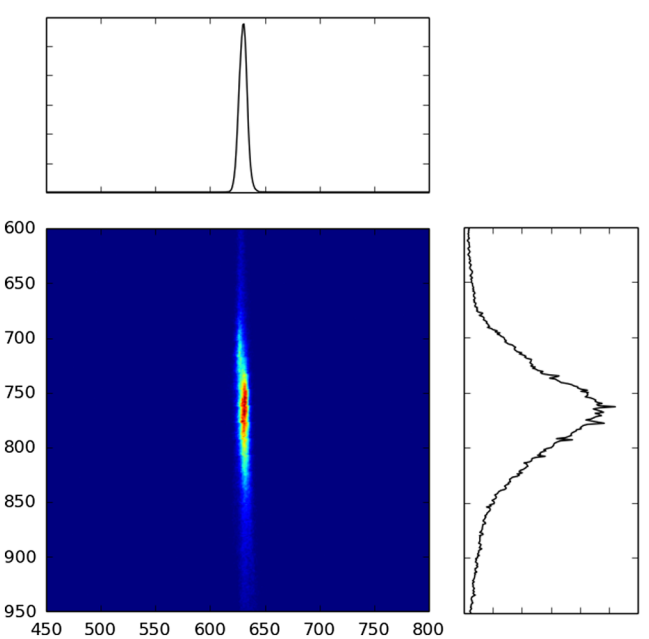

Fig. 10 The SPO focus imaged with PIXI is shown with projections in the dispersion and cross-dispersion directions. The image is plotted in units of PIXI pixels.

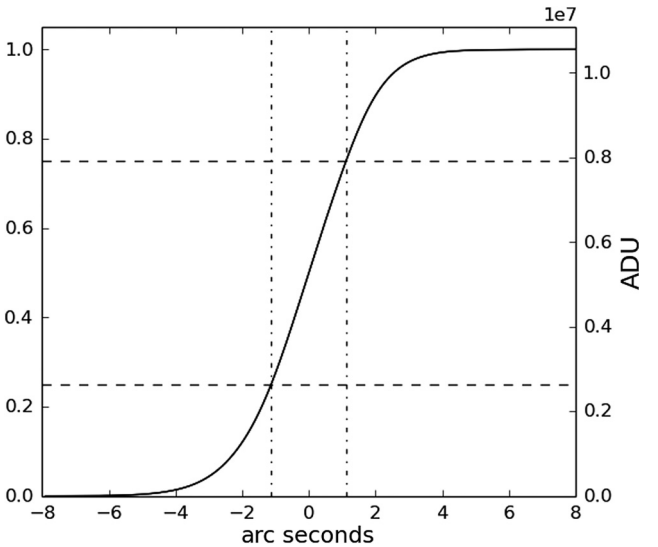

Fig. 11 Spline interpolated cumulative distribution function of the SPO focus. Units on the left y axis are normalized to the sum of the line counts, while units on the right axis are in analog-to-digital units. Vertical dash-dot lines indicate the upper and lower bounds of the half-energy width (HEW).

As noted above, PIXI is not a photon-counting CCD, and images are instead in units of integrated ADU without the availability of a direct conversion to photons. The uncertainty on ADU in each bin does not follow Poisson statistics, and an error based on the (incorrect) assumption of Poisson statistics yields unrealistic uncertainty on the measured HEW of $\lesssim$0.1%. Instead, to estimate its uncertainty, the HEW is calculated individually in each of the subframes of the PIXI integration and the uncertainty is taken as the standard deviation of the HEW over these subframes divided by $\sqrt{n}$, where is the number of subframes (the standard error). For the Mg-K PIXI integration presented here, this procedure is carried out with 19 300 s subframes in the total integration. However, the SPO focus image contains only a single 60 s subframe. Thus, the uncertainty in the HEW cannot be estimated in the same manner, and an uncertainty is not quoted. In order to most directly compare with the single long integration of the SPO focus, the HEW of the Mg-K line is measured from the summed image over all of the 19 subframes.

Figure 12 shows the width of the processed SPO focus in the grating dispersion direction (dashed line) overplotted with the −1st-order Mg-K line (solid line) representing the overall spectrograph focus. The structure of both focuses appears similar, and the HEW of the SPO focus is found to be 2.36 arc seconds, while the HEW of the Mg-K line is found to be 2.15 $\pm$ 0.02 arc seconds. We note that the Mg-K line width may be broader than the calculated line natural line width for an electron impact source. Measurements carried out for the AXAF XSS Electron Impact Point Source suggest that the Mg-K line width may in fact be closer to 1.1 eV. In this case, the line width of Mg-K would be large enough to contribute to the measured HEW of the spectrograph above the uncertainty.

5 Discussion

As a proof of methodology, we have demonstrated a spectrograph composed of SPOs and an aligned off-plane reflection grating module at the PANTER test facility. The LSF of the

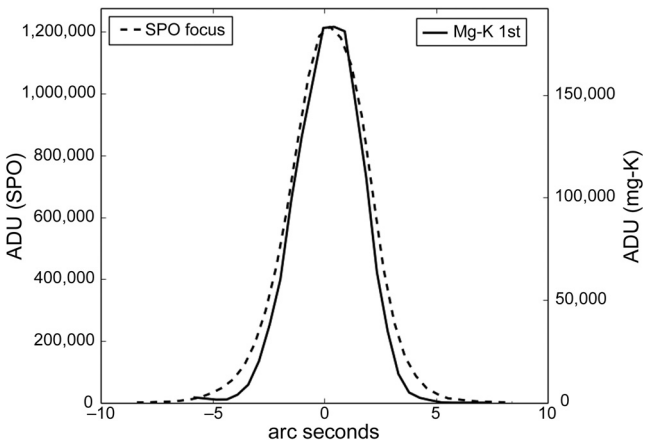

Fig. 12 Mg-K −1st-order PIXI line profile (solid curve) overplotted with the SPO focus line profile (dashed curve). The HEW are found to be 2.36 and 2.15 ± 0.02 arc seconds for the SPO and Mg-K lines, respectively.

spectrograph assembly is characterized by the HEW of the −1st-order Mg-K line. The HEW of the SPO module is measured to be 2.36 arc seconds in the dispersion direction, while the HEW of the spectrograph is measured to be 2.15 ± 0.02 arc seconds. As noted in Sec. 3, previous experimental measurements suggest that the width of the Mg-K line from a target source may be broadened to 1.1 eV (FWHM) compared to the calculated natural line width. In this case, the spectrograph focus would include a non-negligible contribution of 0.62 arc seconds from the line width. Thus, the actual LSF may be as narrow as 2.06 arc seconds. However, we are unable to independently verify the true width of the Mg-K line with the results of this test campaign.

The overall spectrograph Mg-K line width is found to be narrower than that of the SPO. A narrower line width for the spectrograph focus is likely attributable to the grating module subaperturing the light from the SPO in the radial direction. While the SPO focus is an integration over all 13 of the SPO plates, the unmasked regions of the two gratings intercept light from ∼50% of the SPO's azimuthal extent and ∼30% in radius. Thus, any stack error contributions in the SPO will have a relatively larger impact on the width of the SPO focus than on the final spectrograph focus. The spectrograph HEW includes contributions from the telescope figure, telescope alignment, and grating contributions in the form of grating alignment, grating figure, and groove induced aberrations. While we expect grating groove induced aberrations to be small (∼0.5 arc seconds) based on previous measurements,[4] we cannot currently deconvolve these individual contributions. In future tests, a mask would be utilized to stop down the azimuthal extent of the SPO in order to characterize the contributions of the SPO as a function of radius and allow for deconvolution of the telescope and grating contributions.

The performance of the total spectrograph is currently limited by the LSF of the SPO module, which does not yet meet the Arcus resolution requirements. Given the dispersion for this test, $d\lambda/dx = 0.21$ Å/mm, in order to reach the Arcus requirement of $\lambda/\Delta\lambda = 1300$ (FWHM) across the entire instrument bandpass, the spectrograph HEW at Mg-K 1st order must be 18.3 μm, or ∼0.45 arc seconds, at the focal plane. Even in the idealistic case of perfect gratings where the SPO accounted for the entire error budget, the SPO would need to produce an LSF about four times better than the current module. The SPO module focus extent in the dispersion direction is highly dependent on the figure of the SPO plates and on their alignment. Thus, improved performance can be achieved by reducing figure error in the optic. The quality of the forming mandrel is critical to the figure of the final optic. The current SPO test module plates were shaped using a simple aluminum mandrel due to time and budget constraints. In the future, figure quality of the SPO modules will be improved through the use of high-quality polished fused silica mandrels, which have previously been demonstrated by cosine research to produce optics with superior figure.[6]

Acknowledgments

We thank the two referees for their thoughtful comments, which helped to improve this paper. This work was supported by a NASA Earth and Space Science Fellowship (NNX13AM14H), the NASA Roman Technology Fellowship (NNX12AI16G), and a NASA Astrophysics Research and Analysis (APRA) grant (NNX13AD03G). We would also like to acknowledge the support of the University of Iowa Office of the Vice President for Research and the College of Liberal Arts and Sciences.

References

1. R. K. Smith et al., "Arcus: an ISS-attached high-resolution x-ray grating spectrometer," *Proc. SPIE* **9144**, 91444Y (2014).
2. M. Beijersbergen et al., "Silicon pore optics: novel lightweight high-resolution x-ray optics developed for XEUS," *Proc. SPIE* **5488**, 868–874 (2004).
3. V. Burwitz et al., "In focus measurements of IXO type optics using the new PANTER x-ray test facility extension," *Proc. SPIE* **8861**, 88611J (2013).
4. R. McEntaffer et al., "First results from a next-generation off-plane x-ray diffraction grating," *Exp. Astron.* **36**, 389–405 (2013).
5. R. Allured et al., "Optical and x-ray alignment approaches for off-plane reflection gratings," *Proc. SPIE* **9603**, 960315 (2015).
6. R. Willingale et al., "Science requirements and optimization of the silicon pore optics design for the Athena mirror," *Proc. SPIE* **9144**, 91442E (2014).
7. U. G. Briel and E. Pfeffermann, "The position sensitive proportional counter (PSPC) of the Rosat telescope," *Nucl. Instrum. Methods Phys. Res. A* **242**, 376–381 (1986).
8. N. Meidinger et al., "CCD detectors for spectroscopy and imaging of x-rays with the eROSITA space telescope," *Proc. SPIE* **7435**, 743502 (2009).
9. E. Pfeffermann et al., "The focal plane instrumentation of the ROSAT telescope," *Proc. SPIE* **733**, 519–532 (1987).
10. E. Pfeffermann, U. G. Briel, and M. J. Freyberg, "Design and in-orbit-performance of the position sensitive proportional counter onboard the x-ray astronomy satellite ROSAT," *Nucl. Instrum. Methods Phys. Res. A* **515**, 65–69 (2003).
11. J. A. Bearden, "X-ray wavelengths," *Rev. Modern Phys.* **39**, 78–124 (1967).
12. M. O. Krause and J. H. Oliver, "Natural widths of atomic K and L levels, Kα x-ray lines and several KLL Auger lines," *J. Phys. Chem. Ref. Data* **8**, 329–338 (1979).
13. P. H. Citrin et al., "Linewidths in x-ray photoemission and x-ray emission spectroscopies: What do they measure?," *Phys. Rev. B* **10**, 1762–1765 (1974).
14. W. Cash, "X-ray optics—a technique for high resolution imaging," *Appl. Opt.* **26**, 2915–2920 (1987).

Hannah Marlowe received her undergraduate degree in astrophysics from Agnes Scott College in 2011. She is currently a PhD candidate at the University of Iowa and a NASA Earth and Space Science fellow.

Randall L. McEntaffer is an associate professor of physics and astronomy at the University of Iowa. He specializes in the design, fabrication, testing, and implementation of x-ray diffraction gratings for high throughput, high resolving power astrophysical observations. His research topics include the fabrication of x-ray gratings using nanofabrication methodologies, alignment and testing of aligned grating modules, and the incorporation of grating modules into space based spectrometers.

Ryan Allured is the inaugural Leon Van Speybroeck fellow at the Harvard-Smithsonian Center for astrophysics. His research interests span a wide array of instrumentation for astronomical x-ray telescopes. He develops mission concepts for next-generation x-ray observatories as well as the optical technologies to enable such missions. Additionally, he investigates the fundamental optical theories relevant to x-ray optics in order to improve optical performance modeling. He received his PhD in physics from the University of Iowa.

Casey T. DeRoo is a graduate student at the University of Iowa. He received his Bachelor of Arts degree in physics and classical studies from Concordia College in 2011. His current research interests include optical design, manufacture of optics via microfabrication techniques, and x-ray spectroscopy. He is a member of SPIE.

Benjamin D. Donovan is an undergraduate at the University of Iowa, where he works on grating alignment for the off-plane grating rocket experiment (OGRE), a suborbital rocket mission designed to test a high-resolution soft x-ray spectrometer. After he completes his undergraduate degree, he plans on pursuing a graduate degree in astronomy and astrophysics.

Drew M. Miles is an undergraduate at the University of Iowa. His primary research interests are in experimental astrophysics and space instrumentation. After completing his undergraduate curriculum, he will seek to continue his education in a PhD program.

James H. Tutt completed his PhD at the Open University at UK in 2012. He continued at the Open University as a postdoctoral research scholar, working on the use of EM-CCDs in medical imaging before moving to the University of Iowa at USA in 2014. In Iowa, he is working on a suborbital rocket mission that is designed to test a high resolution soft x-ray spectrometer based on EM-CCD cameras and OGRE.

Biographies for the other authors are not available.